EDGE ARTICLE

Check for updates

Fluorescent molecular probe for *in vivo* and *in vitro* targeting and imaging of an intracellular bacterial infection†

Shailendra Koirala, [a] Miguel A. Gaspar, [a] Yalini H. Wijesundara, [a] Dong-Hao Li, [d] Jashkaran G. Gadhvi, [c] Ryanne N. Ehrman, [a] Samuel A. Cornelius, [c] Charles Mariasoosai, [a] Thien-Quang N. Nguyen, [a] Orikeda Trashi, [a] Ikeda Trashi, [a] Sneha Kumari, [a] Laurel M. Hagge, [a] Thomas S. Howlett, [a] Hedieh Torabifard, [a] Bradley D. Smith, [d] Nicole J. De Nisco *[c] and Jeremiah J. Gassensmith *[ab]

Intracellular bacterial infections are difficult to diagnose and treat because the host cells shelter the bacteria from molecular recognition by imaging agents, antibiotics, and the immune system. This problem arises when bladder epithelial cells are infected by uropathogenic *Escherichia coli* (UPEC)—one of the causative agents of urinary tract infection (UTI). UTIs are among the most common bacterial infections and a worldwide health concern. It is challenging to design molecular probes for intracellular UPEC imaging or targeted antibiotic treatment because the probe must possess multiple capabilities—it must permeate the host cell plasma membrane and selectively associate with the intracellular UPEC. Here, we report a "first-in-class" fluorescent probe called BactVue that is comprised of two structural components: a modified zinc(II)-2,2′-dipicolylamine complex (Zn-Oxy-DPA) as the bacteria targeting unit and an appended near-infrared cyanine fluorophore that is hydrophilic but with a near-neutral electrostatic charge. The unique capacity of BactVue to penetrate infected bladder cells and stain intracellular UPEC was demonstrated by a series of *in vitro* and *in vivo* fluorescence imaging studies, including a mouse model of UTI. The results support the feasibility of incorporating BactVue into diagnostic near-infrared fluorescence imaging methods that visualize the location of infected bladder cells during active UTI.

Introduction

Urinary tract infection (UTI) is a common bacterial infection worldwide that can lead to hospitalization in severe cases.[1–5] Women have a 50–60% lifetime occurrence rate of UTI, with 27% of those patients experiencing recurrent episodes. Research has identified uropathogenic *E. coli* (UPEC) as the primary cause of UTIs.[6,7] The ability of UPEC to invade luminal epithelial cells of the bladder (urothelial cells) and avoid inactivation by antibiotics or the host immune system is a critical factor in establishing a persistent infection.[8–10] Recent work has shown that the bacteria invade deep bladder tissues and form intracellular bacterial communities (IBCs) in mice and humans.[4,11,12] These IBCs act as reservoirs that may contribute to frequent recurrence following antibiotic treatment and remission of symptoms.[8,13] Detection of latent intracellular bacteria in a living subject is difficult; consequently, many persistent infections go undiagnosed.[14] Urine culture is commonly used to confirm a UTI; however, this method is relatively slow and resource-intensive, limiting clinical effectiveness as it cannot detect tissue-resident bacteria.[15–18] Faster diagnostic methods, such as urinary dipstick and urine microscopy, have limited diagnostic accuracy and cannot detect intracellular bacteria either.[19–21] Although IBCs are well described, unambiguous identification within living tissue is challenging and remains a major hurdle to clinical translation as—to our knowledge—there are no molecular imaging agents capable of staining bacteria within living cells.

aDepartment of Chemistry and Biochemistry, The University of Texas at Dallas, 800 West Campbell Road, Richardson, Texas 75080-3021, USA. E-mail: gassensmith@utdallas.edu

bDepartment of Biomedical Engineering, The University of Texas at Dallas, 800 West Campbell Road, Richardson, Texas 75080-3021, USA
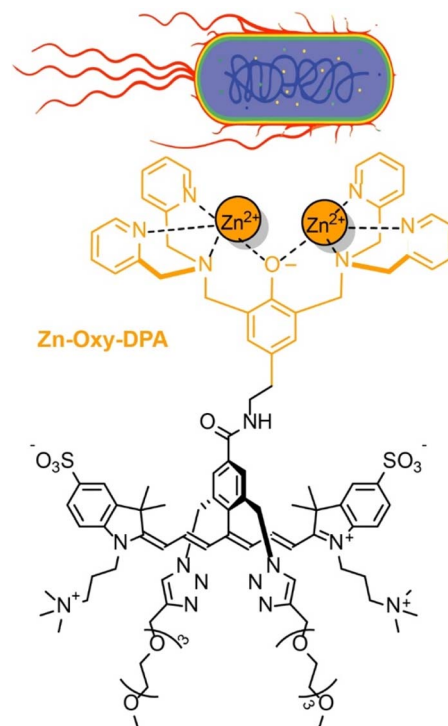
cDepartment of Biological Sciences, The University of Texas at Dallas, 800 West Campbell Road, Richardson, Texas 75080-3021, USA. E-mail: nicole.denisco@utdallas.edu

dDepartment of Chemistry and Biochemistry, University of Notre Dame, 236 Nieuwland Science Hall, Notre Dame, Indiana 46556, USA

The host cell plasma membrane of a living cell is a formidable barrier that protects intracellular bacterial infections such as UTIs, and there is a need for new molecular targeting strategies that enable UTI imaging and treatment.[5,22–24] In principle, the ideal molecule for selective targeting of intracellular UPEC should possess two distinct capabilities—reversibly permeate the cell plasma membrane and selectively associate with the intracellular UPEC. Literature reports of molecules that target intracellular bacteria are rare and focus primarily on antibiotic drug conjugates.[25–28] While large molecules such as antibodies may have attractive molecular recognition properties, their use is likely to be limited by poor membrane permeability. On the other hand, small targeting molecules might exhibit better membrane permeability, but it is challenging to design them with the appropriate cell recognition properties. In this regard, a differentiating feature between healthy mammalian cells and bacteria is the cell surface charge. The surrounding envelope of virtually all bacteria, including UPEC, has an Anionic electrostatic surface, whereas the exterior electrostatic surface of healthy mammalian cell membranes is closer to neutral.[29–31] This difference in surface charge has been exploited by designing cationic molecular probes that have selective affinity for Anionic bacteria membranes. The structural scope includes peptides, synthetic organic molecules, and metal coordination complexes.[32–34] Particularly effective are zinc(ii) 2,2′-dipicolylamine (ZnDPA) coordination complexes, which are known to target Gram-negative and Gram-positive bacteria in complex environments, including living subjects.[29,35,36] The very strong affinity for bacteria is attributed to a synergistic combination of electrostatic attraction and zinc coordination with the abundant Anionic phosphate and carboxylate groups on the polar amphiphiles in the bacterial envelope. In addition to bacteria, ZnDPA complexes are known to target other types of cells with Anionic surfaces, including dead and dying mammalian cells, though this cell surface targeting process does not involve membrane permeation.[37,38] In contrast, a modified version of the ZnDPA scaffold with a bridging oxygen atom between the two zinc(ii) atoms (Zn-Oxy-DPA) is known to readily diffuse through mammalian cell membranes because it can form transient lipophilic ion-pair complexes with the endogenous polar lipids in the plasma membrane.[38–40] We reasoned that a fluorescent Zn-Oxy-DPA probe molecule would become trapped inside an infected bladder cell due to a very strong association with the intracellular bacteria and thus become the basis for fluorescence imaging of UTI (for additional discussion, see ESI† and the computer modeling below).

A key design element is the appended fluorescent dye.[41–44] Near-infrared (NIR) fluorescent dyes are logical choices for *in vivo* imaging owing to the relatively deep tissue penetration of long wavelength light, with minimal background autofluorescence and reduced light scattering by tissue components.[45–52] Heptamethine cyanine (Cy7) dyes possess exceptional NIR fluorescent characteristics; however, because they are naturally hydrophobic, their structures must be modified with charged functional groups to make them water-soluble. This modification is necessary to prevent undesired

Scheme 1 Structure of BactVue. The Zn-Oxy-DPA targeting unit (orange) is attached to a NIR fluorescent Cy7 dye that has a charge-balanced structure with two shielding arms.

processes, such as self-aggregation and non-specific binding to biological surfaces that are not the intended targets.[49,51–53] Since our design goal was a molecular probe that permeated mammalian cells and reached the cytosol, there needed to be a judicious balance of molecular charge and hydrophobicity.[54] This led us to design an NIR fluorescent probe called BactVue (Scheme 1). The molecular structure comprises a Zn-Oxy-DPA targeting unit appended to Cy7 dye with a charge-balanced structure and two short shielding arms.[55–57] We have assessed the capacity of BactVue to target UPEC by conducting a series of *in vitro* and *in vivo* fluorescence imaging studies. We find that BactVue can penetrate infected human bladder cells and stain intracellular UPEC and can be used to visualize UPEC infection within the bladder of a living mouse model of UTI.

Results and discussion

In vitro staining of UTI89 bacteria

BactVue was prepared using a straightforward procedure that covalently connected the Oxy-DPA ligand to the appropriate Cy7 fluorophore (F), followed by treatment with two molar equivalents of Zn(NO$_3$)$_2$ (Fig. 1A). To demonstrate the importance of the charge-neutral characteristic of BactVue, we also prepared an Anionic control dye (Fig. 1B). Both molecular probes were soluble in water. As expected for Cy7 dyes, BactVue exhibited an intense absorption peak at 775 nm with fluorescence emission at 810 nm (Fig. 1C), and the Anionic control dye exhibited very similar spectral properties (Fig. S1†).
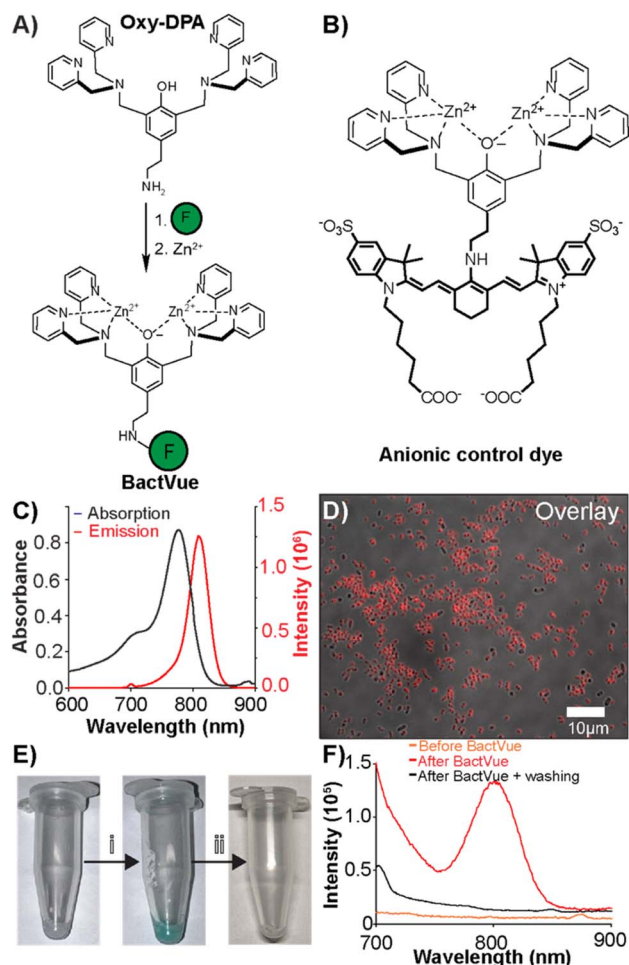
Fig. 1 (A) General synthesis of fluorescent probes. (B) Structure of Anionic control dye. (C) The absorption and emission spectra of BactVue in water (λ_{ex} = 775 nm, λ_{em} = 810 nm). (D) Cy7 fluorescence image of UTI89 bacteria stained with BactVue overlayed with the bright-field image. (E) Images of pelleted liposomes in eppendorf tubes showing BactVue can reversibly associate with cell membranes. The leftmost image shows the pellet before treatment with BactVue, followed by (i) treatment with BactVue, which causes staining, but (ii) after washing, the dye is removed, causing the liposomes to return to their original color. (F) Emission spectrum of before addition of Bact-Vue (orange line) liposomes after incubation with BactVue (red line) and liposomes after washing (black line) showing that BactVue reversibly stains the liposomes.

Initial experiments focused on *in vitro* staining of bacteria and involved the addition of BactVue (final concentration of 10 μM) to a culture of UTI89—a well-characterized laboratory strain of uropathogenic *E. coli*.[58,59] After incubation, the stained bacterial cells were washed three times by repeating a sequence of centrifugation, removal of the aqueous solution, and pellet dispersion in fresh solution. The NIR fluorescence micrograph in Fig. 1D reveals obvious and irreversible BactVue staining of the UTI89 bacteria. An identical staining procedure using Anionic control dye also produced staining of UTI89, as depicted in Fig. S2.† Additional fluorescence imaging evidence was gained by incubating separate UTI89(GFP) samples, a strain of UTI89 that expresses a stable form of green fluorescent protein, with BactVue

or Anionic control dye. In both cases, there was high colocalization of the probe's Cy7 fluorescence with the green emission of the UTI89(GFP) bacteria (Fig. S3†).

High-magnitude microscopy showed that BactVue binds to the outer membrane of *E. coli* (Scheme S4†). Isothermal titration calorimetry was used to evaluate BactVue binding to lipopolysaccharide (LPS), the predominant Anionic lipid in the outer membrane of Gram-negative bacteria. The results (Fig. S4†) demonstrated saturable binding with a biphasic profile, indicating two distinct BactVue binding sites on a single LPS molecule. Analysis revealed K_{D1} at 300 nM and K_{D2} at 1.1 μM. Although further study is needed to clarify the origin of this binding stoichiometry, the nanomolar affinity highlights strong interactions between BactVue and Anionic lipids in bacteria. Given that nearly all bacteria have surface-exposed Anionic phospholipids, we conducted additional experiments and found that BactVue stains other strains of *E. coli*, including *E. coli* CFT703, and other uropathogenic bacterial species, including *Klebsiella pneumoniae* and *Enterococcus faecalis* (Fig. S5†).

The next round of experiments compared the capacity of BactVue and Anionic control dye to permeate liposome bilayers that mimic the plasma membranes of mammalian cells. Unilamellar liposomes (∼250 nm diameter) were prepared with phospholipids that mimic the composition of mammalian plasma membranes (*i.e.*, 98% w/w zwitterionic POPC and 2% w/w Anionic DSPE-PEG2000). Separate samples of liposomes were incubated for 2 h with BactVue and Anionic control dye. After centrifugation and washing, the liposome pellets were examined, and clear differences in their capacity to interact with a lipid bilayer were observed. The liposomes treated with BactVue exhibited a green hue (Fig. S6†), and when the liposomes were resuspended in fresh buffer, fluorescence spectroscopy confirmed the presence of the BactVue (Fig. 1F). In contrast, the pellet of liposomes treated with Anionic control dye was not colored (Fig. S6†) and did not exhibit Cy7 fluorescence when resuspended. These results show that BactVue with charge-neutral fluorophore can favorably interact with a lipid bilayer while the Anionic control dye does not. However, it is equally critical that the probe not become irreversibly trapped in the membrane, as this would prevent its ingress into the cytosol. To that end, we showed that the green color of BactVue-treated liposomes fades significantly after washing with pure buffer and leaves the membrane, returning to the supernatant with each wash (Fig. S6†). This contrasts with the bacterial staining described above, where extensive washing did not dislodge the BactVue probe from the bacterial surface. To unambiguously demonstrate bilayer membrane permeability we prepared Giant Unilamellar Vesicles (GUVs) of the same liposomes using an electroformation technique with a Pt electrode. BactVue was added to the GUVs, incubated, washed, and imaged. Confocal laser scanning microscopy (CLSM) clearly showed that BactVue entered the GUVs and filled the aqueous interior (Fig. S7 and Movies 1–10†).

Computational modeling

To better understand why the Zn-Oxy-DPA targeting unit enables membrane permeation, we conducted steered

molecular dynamics (SMD) simulations of molecular diffusion through a mammalian plasma membrane model. These studies compared two molecules, Zn-Oxy-DPA (BactVue) and ZnDPA, a hypothetical homologous probe that lacks bridging oxygen (see ESI† for the chemical structures). The simulations demonstrated that both molecules interact similarly with the membrane; however, the structure of Zn-Oxy-DPA is more compact and causes less distortion in the bilayer. While both molecules permeate the membrane, Zn-Oxy-DPA does so more efficiently. The bridging oxygen maintains the two Zn cations in a favorable orientation, allowing efficient interaction with the Anionic lipids and facilitating molecular passage through the membrane. In contrast, ZnDPA requires a larger membrane pore to accommodate its more open structure as it maintains a larger distance between its Zn ions during permeation (Fig. S8†). This is corroborated by the change in lipid area per lipid (APL) during simulations, where ZnDPA causes a significant increase in the APL of POPA lipids (Fig. S9†), suggesting it needs more space to permeate.

Further analysis revealed that both molecules undergo conformational changes during membrane permeation. Initially, the molecules were placed in random orientations in the extracellular water at the start of the SMD simulations (Fig. 2A). ZnDPA and Zn-Oxy-DPA approached and interacted

with the membrane similarly, with the primary difference being their orientation at the membrane core and interface regions. The molecules first lay on the membrane surface and interact with the lipid polar head groups (Fig. 2B). Both molecules interacted with lipids such as PLPC and the ceramide lipids NSM and SSM to facilitate membrane entry. For Zn-Oxy-DPA, the molecule penetrated the upper leaflet headgroups and oriented towards the membrane core as a relatively compact structure, whereas the structure of ZnDPA was more disordered and it remained longer at the upper leaflet interface (Fig. 2C and D and Movie S11†).

Additionally, the molecules differed in how they exited the membrane. Zn-Oxy-DPA inverted its orientation to form polar interactions with the membrane headgroups, aiding probe exit from the membrane (Fig. 2F). In contrast, ZnDPA exited directly into the water without significant orientational changes or further membrane interactions. Taken together, the passage of ZnDPA perturbates the membrane significantly more than Zn-Oxy-DPA. In contrast, the compact structure of Zn-Oxy-DPA, stabilized by oxygen-Zn bridging, enables more efficient membrane permeation. Movie S11 in the ESI† compares the entire simulated membrane permeation process for both molecules.

Collectively, the experimental and computational findings indicated that BactVue is a membrane-permeable molecular probe and is likely to enter mammalian cell membranes and bind very strongly to intracellular bacteria; thus, we moved to *in vitro* studies using cell culture.
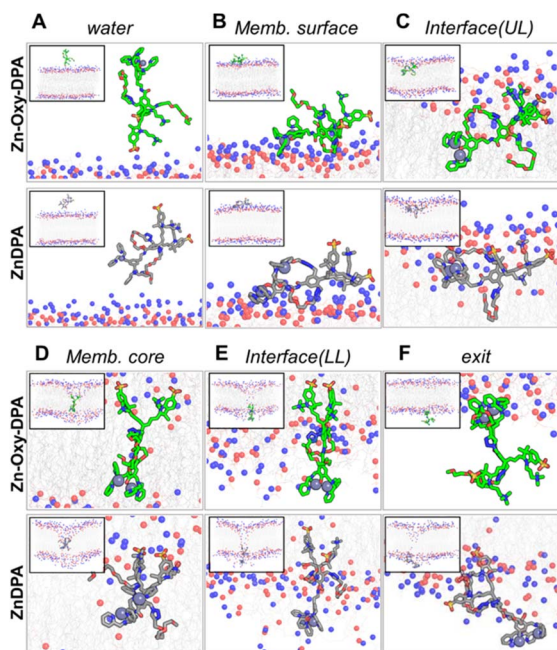

Fig. 2 Representative SMD simulation snapshots of ZnDPA and Zn-Oxy-DPA during their permeation of a model mammalian plasma membrane. Inline images represent the position of the molecules in the membrane bilayer. Conformations of Zn-Oxy-DPA and ZnDPA located at: (A) external membrane water layer, (B) membrane surface, (C) upper leaflet (UL) interface, (D) membrane core, (E) lower leaflet (LL) interface, and (F) internal membrane water layer. ZnOxyDPA and ZnDPA are represented in green and grey colors, respectively. Zn atoms are represented in purple spheres. Lipid headgroup nitrogen and oxygen atoms are represented as blue and red spheres, respectively.
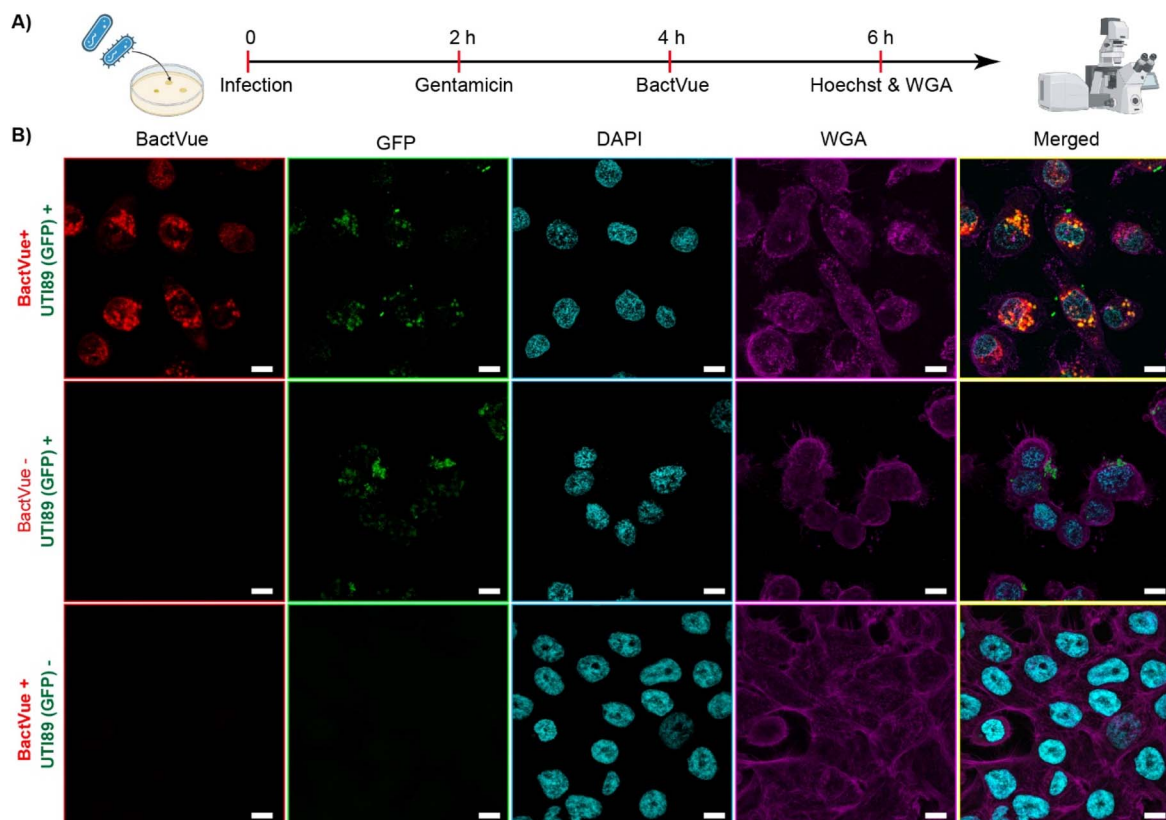
In vitro studies

The first set of *in vitro* imaging cell microscopy experiments examined human 5637 bladder carcinoma cells infected with UTI89(GFP), which enabled unambiguous visualization of the bacteria. The infected bladder cells were treated with gentamicin, an antibiotic that cannot penetrate the bladder cell plasma membrane and thus only kills the extracellular bacteria. Subsequently, the cells were washed repeatedly to ensure the complete removal of any extracellular bacteria and bacterial debris, and the collected supernatant fractions were cultured on CHROMagar plates, which showed no bacterial growth, thereby confirming the effectiveness of gentamicin to kill all extracellular bacteria. The infected bladder cells were sequentially incubated with BactVue for 2 h, washed, fixed, stained with the nuclear stain Hoechst, the cell plasma membrane stain, wheat germ agglutinin (WGA) rhodamine, and imaged using confocal laser scanning microscopy (CLSM). The representative micrographs in Fig. 3B reflect the outcomes of three comparative experiments. In the first row, the human bladder cells were infected with UTI89(GFP), treated with gentamicin to kill extracellular bacteria, and then BactVue was added. In this case, intracellular staining of UTI89(GFP) by BactVue was indicated by a high Pearson colocalization coefficient of 0.72 for the GFP and Cy7 fluorescence. In the second row, bladder cells were infected with UTI89(GFP) and treated with the membrane-impermeable antibiotic gentamicin, but BactVue was not added, and there was no intracellular Cy7 fluorescence. Note

Fig. 3 (A) Schematic illustration of the experiment workflow for staining human 5637 bladder carcinoma cells infected with UTI89(GFP) bacteria. The 5637 bladder cells were infected with UTI89(GFP) (10 bacterial cells per human cell), treated with membrane–impermeable antibiotic gentamicin (100 μg mL^{-1}), washed, treated with BactVue (10 μM), washed, and fixed, treated with Hoechst/WGA rhodamine, washed, and then imaged on a confocal microscope. (B) Confocal imaging: in the first row, cells were infected with UTI89(GFP), treated with gentamicin, and then BactVue was added. In the second row, cells were infected with UTI89(GFP) and treated with gentamicin, and BactVue was not added. In the third row, cells were not infected but treated with gentamicin and BactVue. Hoechst ($\lambda_{ex} = 350$ nm, $\lambda_{em} = 461$ nm), GFP ($\lambda_{ex} = 395$ nm, $\lambda_{em} = 509$ nm), WGA rhodamine ($\lambda_{ex} = 570$ nm, $\lambda_{em} = 590$ nm) and Cy7 ($\lambda_{ex} = 730$ nm, $\lambda_{em} = 779$ nm). Scale bar = 10 μm. Video in ESI (Movie 12–16†).

that some bacteria appear extracellular, though they are enveloped in a cellular membrane—likely a phagocytic cup; thus, these bacteria are 'intracellular'. In the third row, cells were not infected with bacteria but treated with gentamicin and BactVue, and no intracellular Cy7 fluorescence was observed.

To rule out the possibility that our infection was somehow permeabilizing or destabilizing the membrane or that we were staining bacteria on the surface of cells that were then entering the cell, we conducted a control experiment using our Anionic control dye. A sample of human 5637 bladder cells infected with UTI89(GFP) was treated with gentamicin, followed by washing to eliminate all extracellular bacteria. The sample was split into two identical batches, and each batch was separately incubated with BactVue or membrane-impermeable Anionic control dye under the same conditions for 2 h. Following incubation, any extracellular fluorescent probe was removed through washing, and the bladder cells were lysed with 0.1% Triton X-100. The released intracellular bacteria were collected as a pellet after centrifugation, and fluorescence microscopy of the dispersed pellet revealed bacterial staining by BactVue but no bacterial staining by the Anionic control dye (Fig. S10†). These results show that BactVue penetrates the bladder cell membranes and

stains the intracellular bacteria, while the Anionic control dye lacks this capability. In other words, the plasma membrane of the infected bladder cells is sufficiently intact that it prevents permeation of Anionic control dye, which has a polyanionic fluorophore; however, BactVue permeates the plasma membrane, which has the same Zn-Oxy-DPA targeting unit but a charge-neutral fluorophore. Since the anionic control dye stains bacteria just as well as BactVue, it also shows that membrane-bound or "free" bacteria are not being stained and are subsequently taken in by the cells. Taken together, these results show that BactVue uniquely and selectively targets eukaryotic cells harboring intracellular bacteria.

In vivo fluorescence imaging of UTI89 infection in the mouse bladder

The favorable *in vitro* microscopy results motivated us to pursue NIR fluorescence imaging of an *in vivo* model of UTI. The experimental goal was to determine if BactVue could differentiate between infected and non-infected cohorts. Our experimental approach is summarized in Fig. 4A. Nine female BALB/c mice were divided into three groups; groups A and C received intravesical (directly into the bladder) administration of UTI89
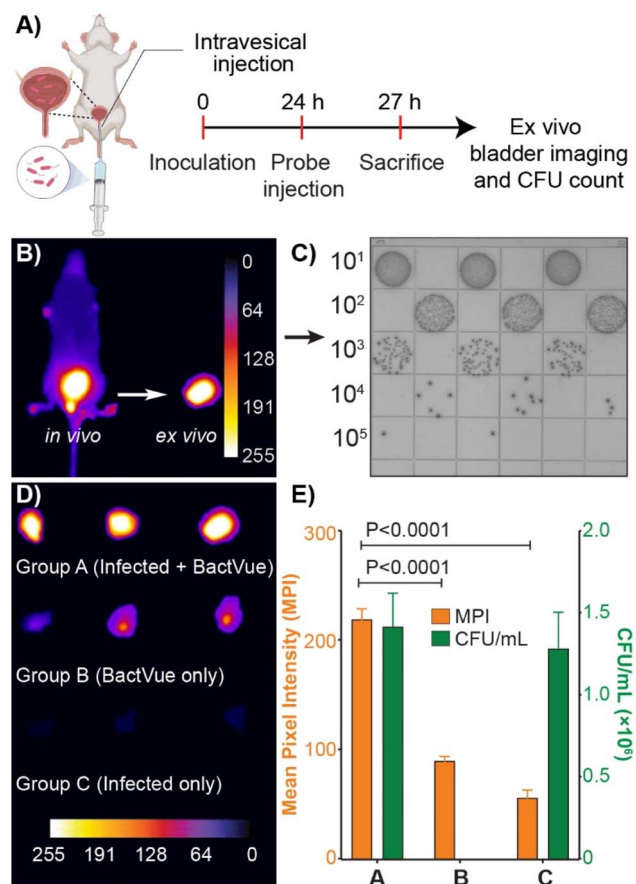
Fig. 4 (A) Schematic illustration of the experiment workflow. (B) *In vivo* and *ex vivo* fluorescence images of a mouse bladder infected with UTI89 (50 μL of 1×10^7 CFU). (C) Bacterial colonies grown from bladder homogenates ($n = 3$) with different dilution factors. (D) *Ex vivo* fluorescence images of three groups of mouse bladders ($n = 3$ for each group) that had been dosed with UTI89 (50 μL of 1×10^7 CFU) or BactVue (50 μL of 50 μM). (E) Quantification of fluorescence and bacteria burden in the three groups of mouse bladders in panel D as fluorescence mean pixel intensity (MPI) or CFU mL^{-1}, respectively ($n = 3$ for each group). A one-way ANOVA determined statistical significance, and the *p*-value was determined by Dunnett's multiple comparison test.

bacteria (50 μL of 1×10^7 CFU) *via* a catheter and were allowed to incubate for 24 h, while group B remained uninfected. Subsequently, groups A and B received intravesical doses of BactVue and live mice were imaged periodically over 3 h. It is worth mentioning that BactVue is sufficiently bright to visualize the infected bladder inside the intact animal and the *ex vivo* bladder (Fig. 4B). *In vivo* fluorescence imaging of the mice in group B (the non-infected group injected with BactVue) revealed a large time-dependent decrease in bladder signal over the 3 h period, reflecting BactVue clearance from the bladder owing to urination (Fig. S12†). In contrast, *in vivo* fluorescence imaging of the mice in group A (infected mice injected with BactVue) exhibited a strong bladder signal that hardly changed over the 3 h period, indicating strong binding and retention of BactVue to the UTI89 bacteria in the bladder (Fig. S12†). After mouse sacrifice, the bladders were extracted for *ex vivo* fluorescence imaging. The bacterial count within each bladder was

determined by homogenizing the bladder tissue, then by plating serially diluted aliquots of homogenate onto CHRO-Magar culture plates and quantifying the CFU mL^{-1}. The bacterial colony data in Fig. S11† confirms that each mouse bladder in group A contained essentially equal counts of UTI89 bacteria. Fluorescent images of the bladders extracted *ex vivo* confirmed the *in vivo* imaging trend, that is, strong retention of the Cy7 fluorescence signal in the bladders of group A mice (infected and treated with BactVue) and decreased fluorescence signal in the group B and C mice (Fig. 4D). Quantification of the *ex vivo* images indicated 2.4 fold higher fluorescence intensity between the infected (group A) and non-infected (group B) mice (Fig. 4E). Statistical analysis confirmed that the difference was highly significant. Though intravesical administration of Bact-Vue would be a clinically useful way to identify and visualize intracellular bacteria, we further demonstrated that BactVue could target infected bladder tissue following tail vein injection. Mice injected with BactVue clearly excreted the dye *via* the urinary tract, where we observed significant fluorescence in the bladders of the infected mice. In contrast, the non-infected mice showed minimal fluorescence (Fig. S13†). Collectively, the *in vivo* and *ex vivo* imaging results show that BactVue can identify infected bladders in a living mouse model of UTI.

Supporting fluorescence microscopy evidence that BactVue selectively targets cells harboring intracellular UTI89 bacteria within infected bladder tissue was gathered by *ex vivo* analysis of the excised bladders using CLSM. An experiment compared two cohorts of female BALB/c mice—the non-infected group *versus* the UTI89-infected group, each $n = 3$. The infected group received an intravesical dose of UTI89 (50 μL of 1×10^7 CFU), whereas the non-infected group received an injection of 0.9% saline. After 24 h, both groups received intravesical injections of BactVue. The mice rested for 3 h and were allowed to drink water and urinate. The mice were sacrificed at that time, and the bladders were extracted. The bladders were longitudinally sectioned (Fig. 5A), stretched with the luminal side facing upwards, fixed, and stained with the nuclear dye Hoechst. The sectioned bladders were imaged using CLSM with multiple fluorescence images stitched together to reconstruct a full-sized image. There was no Cy7 fluorescence signal in the bladders from the non-infected group (Fig. 5C bottom), indicating no retention of BactVue in the bladder tissue. In contrast, there was strong Cy7 fluorescence in localized areas of the bladders from the infected group (Fig. 5C top), indicating retention of BactVue. This interesting result aligns with clinical reports that the bladder infections causing active cystitis are not diffuse dispersions of bacteria, but seem to occur as localized sites of infection distributed around the bladder.[60,61] At higher magnification (Fig. 5D), the BactVue fluorescence appeared as distinctive rod-like and punctate spots, and a stacked 3D reconstruction of the CLSM images revealed the stained bacteria were located within the bladder tissue (see Movie 17 in ESI†). We conclude that BactVue stains intracellular UTI89 bacteria within the mouse bladder epithelium. Thus, BactVue is unique to previously published dyes in its ability to label both extracellular and intracellular bacteria in living bladder tissue.[38]
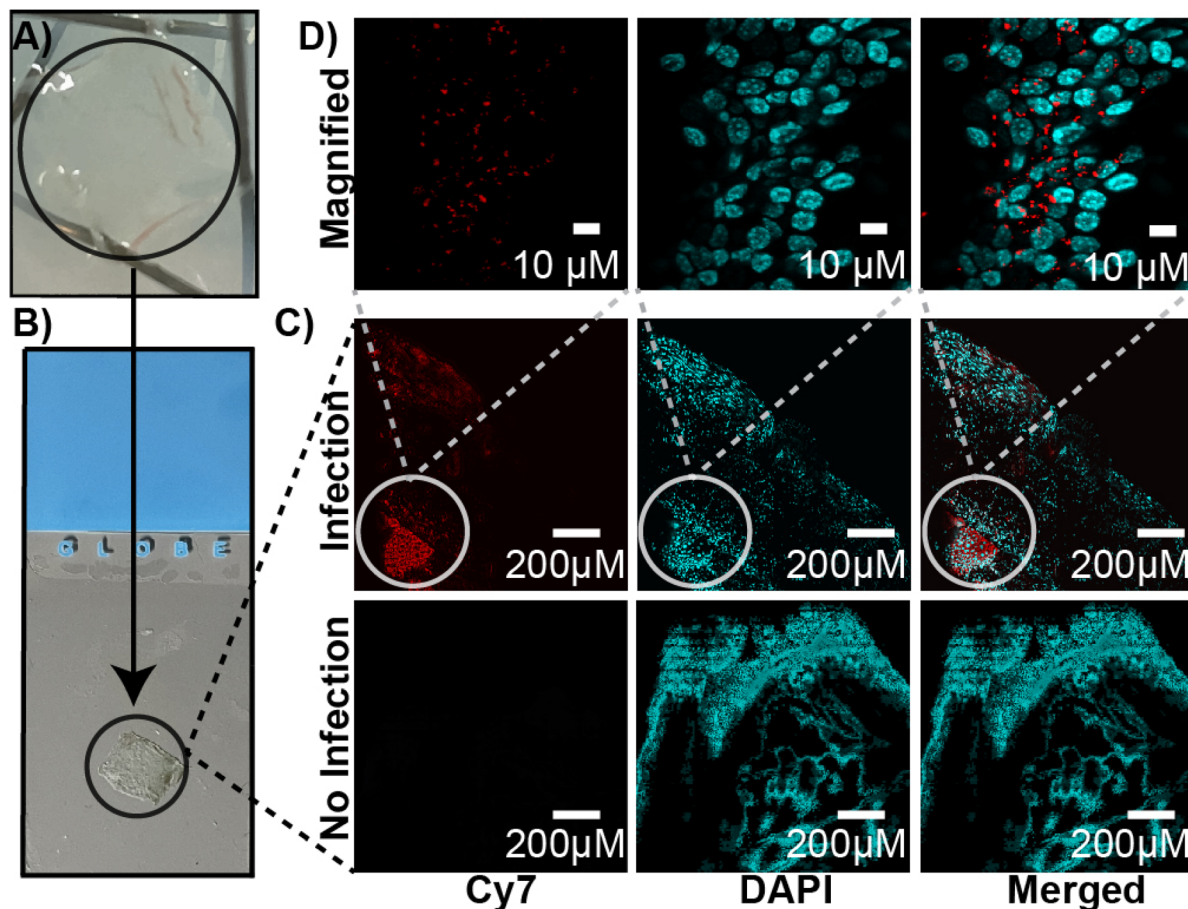
Fig. 5 Images of extracted mouse bladders. Infected mice were given intravesical injections of UTI89 bacteria (50 μL of 1×10^7 CFU) and 24 hours later BactVue (50 μL of a 50 μM solution) was delivered *via* intravesical injection. (A) Stretched mouse bladder lumen on agar bed. (B) Mouse bladder stretched over a microscope slide (C) stitched CLSM images showing fluorescence reconstruction of an entire bladder section from an infected mouse and non-infected mouse, BactVue fluorescence colored red, and Hoechst nuclear fluorescence colored cyan. (D) Magnified CLSM images of the infected mouse bladder in panel (C). Video in ESI (Movies 17 and 18†).

Conclusions

BactVue is the first example of a new class of molecular probes that can target intracellular UPEC within infected bladder cells in cell culture and within a living mouse model of UTI. There is an opportunity to develop new imaging methods that use near-infrared fluorescent BactVue to visualize the location of infected bladder cells within an active UTI. A key molecular design element is the Zn-Oxy-DPA targeting unit, which can diffuse through mammalian cell membranes and strongly bind to intracellular bacteria.[38–40] While this study has focused on one clinical strain of UPEC (*i.e.*, UTI89), it is very likely that BactVue will broadly stain both Gram-negative and Gram-positive bacterial species since the bacterial envelope recognition mechanism is universal. Indeed, we find that BactVue also labels *K. pneumoniae* and *E. faecalis*, the second and third most common bacterial species associated with UTI. Looking to the future, we envision next-generation versions of BactVue that are multi-functional fluorescent probes containing a Zn-Oxy-DPA targeting unit for intracellular UPEC, and an appended peptide motif that is cleaved by bacteria-specific enzymes to produce "turn-on" fluorescence.[62] Another way to exploit the capacity of Zn-Oxy-DPA

to target intracellular UPEC is to synthetically switch the reporter group and create molecular probes for imaging UTI using other modalities such as MRI or PET/SPECT.[32,63] There is also potential to develop therapeutic approaches that exploit the unique targeting capacity of BactVue for image-guided ablation of infected bladder tissue. Light-based therapies using appropriately modified versions of BactVue are particularly attractive since there are already effective clinical methods to illuminate the bladder with light.[64] Moreover, light-based therapies such as photodynamic therapy have the potential to eradicate drug-resistant UPEC, which is often a major factor in the etiology of recurring UTIs.[65,66] We also envision new classes of antibiotic drug conjugates that exploit the selective targeting of intracellular UPEC by the Zn-Oxy-DPA unit. In this regard, it is worth noting that ZnDPA conjugates of antibiotics and anticancer drugs have been reported and found to produce promising therapeutic effects.[67–69]

Data availability

Raw data for the experiments performed can be downloaded from the Open Science Foundation at **https://doi.org/10.17605/OSF.IO/G97A5**. Structure inputs, parameter files, and

representative trajectory of the simulation can be found in a Zenodo repository. Zenodo URL: https://zenodo.org/records/15097014 DOI: 10.5281/zenodo.15097013.

Author contributions

Conflicts of interest

The authors declare that they have no competing interests.

Acknowledgements

References

1 B. Foxman, The epidemiology of urinary tract infection, *Nat. Rev. Urol.*, 2010, **7**, 653–660.

2 M. Medina and E. Castillo-Pino, An introduction to the epidemiology and burden of urinary tract infections, *Ther. Adv. Urol.*, 2019, **11**, DOI: 10.1177/1756287219832172.

3 A. Al-Badr and G. Al-Shaikh, Recurrent Urinary Tract Infections Management in Women: a review, *Sultan Qaboos Univ. Med. J.*, 2013, **13**, 359–367.

4 A. L. Flores-Mireles, J. N. Walker, M. Caparon and S. J. Hultgren, Urinary tract infections: epidemiology, mechanisms of infection and treatment options, *Nat. Rev. Microbiol.*, 2015, **13**, 269–284.

5 M. A. Luzuriaga, F. C. Herbert, O. R. Brohlin, J. Gadhvi, T. Howlett, A. Shahrivarkevishahi, Y. H. Wijesundara, S. Venkitapathi, K. Veera, R. Ehrman, C. E. Benjamin, S. Popal, M. D. Burton, M. A. Ingersoll, N. J. De Nisco and J. J. Gassensmith, Metal–Organic Framework Encapsulated Whole-Cell Vaccines Enhance Humoral Immunity against Bacterial Infection, *ACS Nano*, 2021, **15**, 17426–17438.

6 M. Totsika, D. G. Moriel, A. Idris, B. A. Rogers, D. J. Wurpel, M. D. Phan, D. L. Paterson and M. A. Schembri, Uropathogenic *Escherichia coli* mediated urinary tract infection, *Curr. Drug Targets*, 2012, **13**, 1386–1399.

7 C. Shah, R. Baral, B. Bartaula and L. B. Shrestha, Virulence factors of uropathogenic *Escherichia coli* (UPEC) and correlation with antimicrobial resistance, *BMC Microbiol.*, 2019, **19**, 204.

8 Y. Liu, Y. Jia, K. Yang and Z. Wang, Heterogeneous Strategies to Eliminate Intracellular Bacterial Pathogens, *Front. Microbiol.*, 2020, **11**, 563.

9 T. J. Hannan, M. Totsika, K. J. Mansfield, K. H. Moore, M. A. Schembri and S. J. Hultgren, Host-pathogen checkpoints and population bottlenecks in persistent and intracellular uropathogenic *Escherichia coli* bladder infection, *FEMS Microbiol. Rev.*, 2012, **36**, 616–648.

10 S. Venkitapathi, Y. H. Wijesundara, S. A. Cornelius, F. C. Herbert, J. J. Gassensmith, P. E. Zimmern and N. J. De Nisco, Conserved FimK Truncation Coincides with Increased Expression of Type 3 Fimbriae and Cultured Bladder Epithelial Cell Association in Klebsiella quasipneumoniae, *J. Bacteriol.*, 2022, **204**, e0017222.

11 G. G. Anderson, K. W. Dodson, T. M. Hooton and S. J. Hultgren, Intracellular bacterial communities of uropathogenic *Escherichia coli* in urinary tract pathogenesis, *Trends Microbiol.*, 2004, **12**, 424–430.

12 N. J. De Nisco, M. Neugent, J. Mull, L. Chen, A. Kuprasertkul, M. de Souza Santos, K. L. Palmer, P. Zimmern and K. Orth, Direct Detection of Tissue-Resident Bacteria and Chronic Inflammation in the Bladder Wall of Postmenopausal Women with Recurrent Urinary Tract Infection, *J. Mol. Biol.*, 2019, **431**, 4368–4379.

13 J. M. Bower, D. S. Eto and M. A. Mulvey, Covert operations of uropathogenic *Escherichia coli* within the urinary tract, *Traffic*, 2005, **6**, 18–31.

14 G. C. Ulett, M. Totsika, K. Schaale, A. J. Carey, M. J. Sweet and M. A. Schembri, Uropathogenic *Escherichia coli* virulence and innate immune responses during urinary tract infection, *Curr. Opin. Microbiol.*, 2013, **16**, 100–107.

15 R. Xu, N. Deebel, R. Casals, R. Dutta and M. Mirzazadeh, A New Gold Rush: A Review of Current and Developing Diagnostic Tools for Urinary Tract Infections, *Diagnostics*, 2021, **11**, 479.

16 A. Masajtis-Zagajewska and M. Nowicki, New markers of urinary tract infection, *Clin. Chim. Acta*, 2017, **471**, 286–291.

17 C. M. Chu and J. L. Lowder, Diagnosis and treatment of urinary tract infections across age groups, *Am. J. Obstet. Gynecol.*, 2018, **219**, 40–51.

18 G. Schmiemann, E. Kniehl, K. Gebhardt, M. M. Matejczyk and E. Hummers-Pradier, The diagnosis of urinary tract infection: a systematic review, *Dtsch Arztebl. Int.*, 2010, **107**, 361–367.

19 S. Najeeb, T. Munir, S. Rehman, A. Hafiz, M. Gilani and M. Latif, Comparison of urine dipstick test with conventional urine culture in diagnosis of urinary tract infection, *J. Coll. Physicians Surg. Pak.*, 2015, **25**, 108–110.

20 I. Dadzie, E. Quansah, M. Puopelle Dakorah, V. Abiade, E. Takyi-Amuah and R. Adusei, The Effectiveness of Dipstick for the Detection of Urinary Tract Infection, *Can. J. Infect. Dis. Med. Microbiol.*, 2019, **2019**, 8642628.

21 M. Fritzenwanker, C. Imirzalioglu, T. Chakraborty and F. M. Wagenlehner, Modern diagnostic methods for urinary tract infections, *Expert Rev. Anti-Infect. Ther.*, 2016, **14**, 1047–1063.

22 R. E. Berry, D. J. Klumpp and A. J. Schaeffer, Urothelial cultures support intracellular bacterial community formation by uropathogenic *Escherichia coli*, *Infect. Immun.*, 2009, **77**, 2762–2772.

23 V. C. Scott, D. A. Haake, B. M. Churchill, S. S. Justice and J. H. Kim, Intracellular Bacterial Communities: A Potential Etiology for Chronic Lower Urinary Tract Symptoms, *Urology*, 2015, **86**, 425–431.

24 G. G. Anderson, S. M. Martin and S. J. Hultgren, Host subversion by formation of intracellular bacterial communities in the urinary tract, *Microbes Infect.*, 2004, **6**, 1094–1101.

25 S. M. Lehar, T. Pillow, M. Xu, L. Staben, K. K. Kajihara, R. Vandlen, L. DePalatis, H. Raab, W. L. Hazenbos, J. H. Morisaki, J. Kim, S. Park, M. Darwish, B. C. Lee, H. Hernandez, K. M. Loyet, P. Lupardus, R. Fong, D. Yan, C. Chalouni, E. Luis, Y. Khalfin, E. Plise, J. Cheong, J. P. Lyssikatos, M. Strandh, K. Koefoed, P. S. Andersen, J. A. Flygare, M. Wah Tan, E. J. Brown and S. Mariathasan, Novel antibody-antibiotic conjugate eliminates intracellular *S. aureus*, *Nature*, 2015, **527**, 323–328.

26 Y. Jiang, M. Han, Y. Bo, Y. Feng, W. Li, J. R. Wu, Z. Song, Z. Zhao, Z. Tan, Y. Chen, T. Xue, Z. Fu, S. H. Kuo, G. W. Lau, E. Luijten and J. Cheng, "Metaphilic" Cell-Penetrating Polypeptide-Vancomycin Conjugate Efficiently Eradicates Intracellular Bacteria *via* a Dual Mechanism, *ACS Cent. Sci.*, 2020, **6**, 2267–2276.

27 A. Kuroki, A. Kengmo Tchoupa, M. Hartlieb, R. Peltier, K. E. S. Locock, M. Unnikrishnan and S. Perrier, Targeting intracellular, multi-drug resistant Staphylococcus aureus with guanidinium polymers by elucidating the structure-activity relationship, *Biomaterials*, 2019, **217**, 119249.

28 E. K. Lei, M. P. Pereira and S. O. Kelley, Tuning the intracellular bacterial targeting of peptidic vectors, *Angew Chem. Int. Ed. Engl.*, 2013, **52**, 9660–9663.

29 D. R. Rice, K. J. Clear and B. D. Smith, Imaging and therapeutic applications of zinc(ii)-dipicolylamine molecular probes for anionic biomembranes, *Chem. Commun.*, 2016, **52**, 8787–8801.

30 P. Li, C. Zhou, S. Rayatpisheh, K. Ye, Y. F. Poon, P. T. Hammond, H. Duan and M. B. Chan-Park, Cationic peptidopolysaccharides show excellent broad-spectrum antimicrobial activities and high selectivity, *Adv. Mater.*, 2012, **24**, 4130–4137.

31 R. G. Hanshaw, S. M. Hilkert, H. Jiang and B. D. Smith, An indicator displacement system for fluorescent detection of phosphate oxyanions under physiological conditions, *Tetrahedron Lett.*, 2004, **45**, 8721–8724.

32 T. A. Aweda, Z. F. B. Muftuler, A. V. F. Massicano, D. Gadhia, K. A. McCarthy, S. Queern, A. Bandyopadhyay, J. Gao and S. E. Lapi, Radiolabeled Cationic Peptides for Targeted Imaging of Infection, *Contrast Media Mol. Imaging*, 2019, **2019**, 3149249.

33 Y. Ji, G. Li, J. Wang, C. Piao and X. Zhou, Recent Progress in Identifying Bacteria with Fluorescent Probes, *Molecules*, 2022, **27**, 6440.

34 J. Jiou, K. Chiravuri, A. Gudapati and J. J Gassensmith, The Chemistry of Confined Spaces, *Curr. Org. Chem.*, 2014, **18**, 2002–2009.

35 H. T. Ngo, X. Liu and K. A. Jolliffe, Anion recognition and sensing with Zn(ii)-dipicolylamine complexes, *Chem. Soc. Rev.*, 2012, **41**, 4928–4965.

36 W. MattheaLeevy, Selective recognition of bacterial membranes by zinc(ii)-coordination complexes, *Chem. Commun.*, 2006, 1595–1597.

37 C. Lakshmi, R. G. Hanshaw and B. D. Smith, Fluorophore-linked zinc(ii) dipicolylamine coordination complexes as sensors for phosphatidylserine-containing membranes, *Tetrahedron*, 2004, **60**, 11307–11315.

38 K. J. Clear, K. M. Harmatys, D. R. Rice, W. R. Wolter, M. A. Suckow, Y. Wang, M. Rusckowski and B. D. Smith, Phenoxide-Bridged Zinc(ii)-Bis(dipicolylamine) Probes for Molecular Imaging of Cell Death, *Bioconjugate Chem.*, 2016, **27**, 363–375.

39 K. M. DiVittorio, W. M. Leevy, E. J. O'Neil, J. R. Johnson, S. Vakulenko, J. D. Morris, K. D. Rosek, N. Serazin, S. Hilkert and S. Hurley, Zinc(ii) coordination complexes as membrane-active fluorescent probes and antibiotics, *ChemBioChem*, 2008, **9**, 286–293.

40 H. Jiang, J. O'Neil E, K. M. Divittorio and B. D. Smith, Anion-mediated phase transfer of Zinc(ii)-coordinated tyrosine derivatives, *Org. Lett.*, 2005, **7**, 3013–3016.

41 M. Savastano, M. Fiaschi, G. Ferraro, P. Gratteri, P. Mariani, A. Bianchi and C. Bazzicalupi, Sensing Zn(2+) in Aqueous Solution with a Fluorescent Scorpiand Macrocyclic Ligand Decorated with an Anthracene Bearing Tail, *Molecules*, 2020, **25**, 1355.

42 M. J. Ruedas-Rama and E. A. Hall, Azamacrocycle activated quantum dot for zinc ion detection, *Anal. Chem.*, 2008, **80**, 8260–8268.

43 T. Ahmad, A. Waheed, S. Abdel-Azeim, S. Khan and N. Ullah, Three new turn-on fluorescent sensors for the selective detection of Zn^{2+}: synthesis, properties and DFT studies, *Arabian J. Chem.*, 2022, **15**, 104002.

44 N. Dash, A. Malakar, M. Kumar, B. B. Mandal and G. Krishnamoorthy, Metal ion dependent "ON" intramolecular charge transfer (ICT) and "OFF" normal switching of the fluorescence: sensing of Zn^{2+} by ICT emission in living cells, *Sens. Actuators, B*, 2014, **202**, 1154–1163.

45 S. M. Usama, S. C. Marker, S. Hernandez Vargas, S. AghaAmiri, S. C. Ghosh, N. Ikoma, H. S. Tran Cao, M. J. Schnermann and A. Azhdarinia, Targeted Dual-Modal PET/SPECT-NIR Imaging: From Building Blocks and Construction Strategies to Applications, *Cancers*, 2022, **14**, 1619.

46 K. Welsher, S. P. Sherlock and H. Dai, Deep-tissue anatomical imaging of mice using carbon nanotube fluorophores in the second near-infrared window, *Proc. Natl. Acad. Sci. U. S. A.*, 2011, **108**, 8943–8948.

47 S. G. Demos, R. Gandour-Edwards, R. Ramsamooj and R. White, Near-infrared autofluorescence imaging for detection of cancer, *J. Biomed. Opt.*, 2004, **9**, 587–592.

48 C. Paras, M. Keller, L. White, J. Phay and A. Mahadevan-Jansen, Near-infrared autofluorescence for the detection of parathyroid glands, *J. Biomed. Opt.*, 2011, **16**, 067012.

49 D. H. Li, R. S. Gamage, A. G. Oliver, N. L. Patel, S. Muhammad Usama, J. D. Kalen, M. J. Schnermann and B. D. Smith, Doubly Strapped Zwitterionic NIR-I and NIR-II Heptamethine Cyanine Dyes for Bioconjugation and Fluorescence Imaging, *Angew Chem. Int. Ed. Engl.*, 2023, **62**, e202305062.

50 A. Shahrivarkevishahi, M. A. Luzuriaga, F. C. Herbert, A. C. Tumac, O. R. Brohlin, Y. H. Wijesundara, A. V. Adlooru, C. Benjamin, H. Lee, P. Parsamian, J. Gadhvi, N. J. De Nisco and J. J. Gassensmith, PhotothermalPhage: A Virus-Based Photothermal Therapeutic Agent, *J. Am. Chem. Soc.*, 2021, **143**, 16428–16438.

51 Y.-T. Long and T. J. Meade, Advances in optical and electrochemical techniques for biomedical imaging, *Chem. Sci.*, 2020, **11**, 6940–6941.

52 C. J. Adams, R. Krueger and T. J. Meade, A multimodal Ca(II) responsive near IR-MR contrast agent exhibiting high cellular uptake, *ACS Chem. Biol.*, 2020, **15**, 334–341.

53 D. H. Li, R. S. Gamage and B. D. Smith, Sterically Shielded Hydrophilic Analogs of Indocyanine Green, *J. Org. Chem.*, 2022, **87**, 11593–11601.

54 N. J. Yang and M. J. Hinner, Getting across the cell membrane: an overview for small molecules, peptides, and proteins, *Methods Mol. Biol.*, 2015, **1266**, 29–53.

55 E. J. O'Neil and B. D. Smith, Anion recognition using dimetallic coordination complexes, *Coord. Chem. Rev.*, 2006, **250**, 3068–3080.

56 D. H. Li, C. L. Schreiber and B. D. Smith, Sterically Shielded Heptamethine Cyanine Dyes for Bioconjugation and High Performance Near-Infrared Fluorescence Imaging, *Angew Chem. Int. Ed. Engl.*, 2020, **59**, 12154–12161.

57 D. Li, *Structural Optimization of Heptamethine Cyanine Dyes*, University of Notre Dame, 2022.

58 R. Kulkarni, B. K. Dhakal, E. S. Slechta, Z. Kurtz, M. A. Mulvey and D. G. Thanassi, Roles of putative type II secretion and type IV pilus systems in the virulence of uropathogenic *Escherichia coli*, *PLoS One*, 2009, **4**, e4752.

59 K. J. Wright, P. C. Seed and S. J. Hultgren, Development of intracellular bacterial communities of uropathogenic *Escherichia coli* depends on type 1 pili, *Cell. Microbiol.*, 2007, **9**, 2230–2241.

60 J. A. Vazquez and J. D. Sobel, in *Essentials of clinical mycology*, Springer, 2010, pp. 167–206.

61 P. M. Hanno, Interstitial cystitis and related disorders, *Campbell's urology*, 2002, vol. 1, pp. 631–670.

62 E. Y. H. Xin, G. Kwek, X. An, C. Sun, S. Liu, N. S. Qing, S. Lingesh, L. Jiang, G. Liu and B. Xing, Enzymes in Synergy: Bacteria Specific Molecular Probe for Locoregional Imaging of Urinary Tract Infection *in vivo*, *Angew. Chem.*, 2024, **136**, e202406843.

63 H. Lee, A. Shahrivarkevishahi, J. L. Lumata, M. A. Luzuriaga, L. M. Hagge, C. E. Benjamin, O. R. Brohlin, C. R. Parish, H. R. Firouzi, S. O. Nielsen, L. L. Lumata and J. J. Gassensmith, Supramolecular and biomacromolecular enhancement of metal-free magnetic resonance imaging contrast agents, *Chem. Sci.*, 2020, **11**, 2045–2050.

64 C. C. Evelyne, J. J. de La Rosette and T. M. de Reijke, Emerging optical techniques in advanced cystoscopy for bladder cancer diagnosis: a review of the current literature, *Indian J. Urol.*, 2011, **27**, 245–251.

65 Y. Y. Huang, A. Wintner, P. C. Seed, T. Brauns, J. A. Gelfand and M. R. Hamblin, Antimicrobial photodynamic therapy mediated by methylene blue and potassium iodide to treat urinary tract infection in a female rat model, *Sci. Rep.*, 2018, **8**, 7257.

66 D. Tichaczek-Goska, M. Glensk and D. Wojnicz, The Enhancement of the Photodynamic Therapy and Ciprofloxacin Activity against Uropathogenic *Escherichia coli* Strains by Polypodium vulgare Rhizome Aqueous Extract, *Pathogens*, 2021, **10**, 1544.

67 V. Yarlagadda, P. Sarkar, S. Samaddar, G. B. Manjunath, S. D. Mitra, K. Paramanandham, B. R. Shome and J. Haldar, Vancomycin Analogue Restores Meropenem Activity against NDM-1 Gram-Negative Pathogens, *ACS Infect. Dis.*, 2018, **4**, 1093–1101.

68 D. Guan, F. Chen, Faridoon, J. Liu, J. Li, L. Lan and W. Huang, Design and Synthesis of Pyrophosphate-Targeting Vancomycin Derivatives for Combating Vancomycin-Resistant Enterococci, *ChemMedChem*, 2018, **13**, 1644–1657.

69 Y. W. Liu, Y. Y. Chen, C. Y. Hsu, T. Y. Chiu, K. L. Liu, C. F. Lo, M. Y. Fang, Y. C. Huang, T. K. Yeh, K. Y. Pak, B. D. Gray, T. A. Hsu, K. H. Huang, C. Shih, K. S. Shia, C. T. Chen and L. K. Tsou, Linker Optimization and Therapeutic Evaluation of Phosphatidylserine-Targeting Zinc Dipicolylamine-based Drug Conjugates, *J. Med. Chem.*, 2019, **62**, 6047–6062.